Anodic TiO_2 nanotubes decorated by Pt nanoparticles using ALD: An efficient electrocatalyst for methanol oxidation

V. C Anitha[a], Raul Zazpe[a,d], Milos Krbal[a], JeongEun Yoo[b], Hanna Sopha[a,d], Jan Prikryl[a], Gihoon Cha[b], Stanislav Slang[a], Patrik Schmuki[b,c], Jan M. Macak[a,d,*]

[a] Center of Materials and Nanotechnologies, Faculty of Chemical Technology, University of Pardubice, Nam. Cs. Legii 565, 53002 Pardubice, Czech Republic.
[b] Department of Materials Science, Institute for Surface Science and Corrosion WW4-LKO, Friedrich-Alexander University, Martensstraße 7, D-91058 Erlangen, Germany.
[c] Chemistry Department, Faculty of Sciences, King Abdulaziz University, 80203 Jeddah, Saudi Arabia Kingdom
[d] Central European Institute of Technology, Brno University of Technology, Purkynova 123, 61200 Brno, Czech Republic

*Corresponding author: Tel: +420 466037 401, E-mail: jan.macak@upce.cz (J.M. Macak)

Abstract

Anodic TiO_2 nanotube layers (TNTs) of different thicknesses (≈ 1, 5 and 20 µm) were homogeneously decorated with Pt nanoparticles using atomic layer deposition (ALD) and explored for the electrocatalytic activity in methanol oxidation reaction (MOR). Six different numbers of ALD cycles (N_{ALD}) - 24, 40, 56, 72, 88 and 104 - were used. Pt nanoparticles with diameter in the range of 1.3 to 4.6 nm were obtained for the first five N_{ALD} and a complete coating was achieved for the highest N_{ALD} (104). The SEM/TEM analyses revealed that Pt nanoparticles uniformly decorated exteriors and interiors of TNTs. A linear increase of the particle diameter of Pt was revealed with increasing N_{ALD}. Highest electrocatalytic activities of Pt/TNTs electrodes represented by current density of 74 mA/cm^2 were obtained for N_{ALD} = 88 and for thickest TNTs (20 µm). The electrooxidation performance of Pt-decorated TiO_2 nanotube layers was thoroughly compared to reference substrates: Pt-decorated graphite sheets and TiO_2 flat layers (on annealed Ti foils) as well as for a commercial Pt/C catalyst attached on graphite sheets. From chronoamperometric measurements it turned out that the catalytic activity of Pt-

loaded nanotube layers is superior and long lasting compared to other substrates, where significant degree of catalyst poisoning takes place. The presented ALD decoration approach is an effective strategy for the homogeneous distribution of precious Pt nanoparticles on a high surface area catalyst support for high-performance electrocatalysis.

Key words: TiO_2 nanotubes, Pt nanoparticles, atomic layer deposition, electrocatalysis, methanol electrooxidation

1. Introduction

The new generation of fuel cells based on direct electrooxidation of alcohols is an attractive alternative for the production of energy [1, 2]. Direct methanol fuel cells (DMFCs) are effective electrochemical devices that have been receiving extensive attention due to their simplicity and operation for portable devices [3, 4]. In addition, DMFCs have several advantages such as high-energy conversion efficiency, low operating cost/temperature, low weight, use of liquid fuel and long operation life [5, 6]. In DMFCs, there are two basic chemical reactions involved: (i) the anode side-methanol oxidation reaction (MOR) and (ii) the cathode side- oxygen reduction reaction (ORR) [5, 7]. This study focuses on the anode side, which is the site of MOR. In methanol oxidation, methanol is electrooxidized into CO_2 and six electrons per methanol molecule and making it as a promising fuel in DMFCs [8].

Generally, nano-structured platinum (Pt) is used as an electrocatalysts for MOR in DMFCs due to its greater catalytic activity than other noble metals [6, 9]. Practically, because of the high price of Pt, the catalytic Pt nanoparticles are dispersed on a high surface area conductive support/carrier material to attain best catalyst utilization and performance [10]. However, the

achievement of well-dispersed Pt nanoparticles with controlled particle size, distribution, and accommodation on a proper support material represent challenges for their large-scale applications. Moreover, the catalytic efficiency is limited by the slow oxidation kinetics of methanol and carbon monoxide (CO, by-product) poisoning effect [6, 7, 11, 12]. To address these problems, great efforts have been made over the past decades, in which the selection of a support/carrier for Pt catalyst represents one of the key steps to improve the dispersion of Pt nanoparticles and solve aggregation problems [6, 7, 13, 14]. The catalyst support can further strongly influence the activity of the metallic Pt nanoparticles via metal-support interactions [15-17]. As commonly used catalyst support in DMFC, carbon-based materials suffer from corrosion and weak interaction between catalysts and support resulting in severe agglomeration of catalysts under reaction conditions and a decrease of the durability and stability of the catalyst itself [18-20]. Therefore, the synthesis of an ideal support material with well dispersed/stable catalyst surface is one of the present goals in the field of DMFCs.

Self-organized TiO_2 nanotubes (TNTs) produced by anodization of a Ti substrate represent great choice as catalyst support owing to their strong catalyst-support interaction [16, 17, 21], high ordering [22], good stability in the fuel cell operation conditions [23], and large internal surface area [24, 25], which are very useful for an effective dispersion of the precious Pt-loading content. The feasibility of fast charge propagation within TNTs and the existence of the mutual metal-support interactions are facilitated because of the direct connection between self-organized TNTs and Ti substrate. In addition, anodization is a simple and low cost electrochemical approach, and offers a great control of the nanotube size/morphology.

Recently, the combination of anodic TNTs and Pt nanoparticles for various catalytic applications has been reported [26-33]. Several approaches are described in the literature for Pt

catalysts deposition on TNTs that have various dimensions and morphologies such as chemical impregnation [26], electrodeposition [27], immobilization [28], photo-assisted reduction [29, 30], thermal decomposition [31], anodization of Ti-Pt alloy [32] and thermal de-wetting of sputter coated Pt [33]. On the other hand, alloying Pt with other metals, such as Ru [28, 34, 35] and Pd [36, 37], is a typical route to reduce the CO poisoning effect and enhance the electrocatalytic activity. However, in most of the studies, the Pt and alloyed nanostructures are synthesized through solution routes and further immobilization on the support material. In addition, catalysts synthesized by solution routes have some disadvantages, namely, utilization of surfactants that are used to stabilize the particles and to avoid their agglomeration during the process. Moreover, some reproducibility issues due to the difficulty in control of reaction conditions may occur for these processes. These drawbacks can be overcome by the use of atomic layer deposition (ALD) to deposit catalytic nanoparticles of noble metals such as Pt [38-42], Au [43, 44] or Pd [38, 45, 46] on various supports for different electrocatalytic applications, a key being the excellent homogeneity and quality of the particles. ALD is a deposition technique that uses gaseous precursor as material sources for film or particle deposition and offers additional benefits such as high conformality regardless of substrate's shape and precise size/thickness/composition control of the deposited material.

The aim of the present study is to exploit anodic TNT layers with different thicknesses as a catalyst support for uniformly decorated Pt nanoparticles using ALD towards an efficient catalyst for methanol electrooxidation.

2. Experimental

2.1 Fabrication of self-organized TiO_2 nanotube layers

Self-organized TiO_2 nanotube layers (TNTs) with different thicknesses (1, 5, 20 μm) were fabricated on Ti foils via anodization. Prior to anodization, Ti foils (Sigma-Aldrich, 0.127 mm thickness, 99.7 % purity) were degreased by sonication in isopropanol and acetone followed by rinsing with isopropanol and drying in air. Anodization of the foils was carried out at room temperature employing a high-voltage potentiostat (PGU-200V, IPS Elektroniklabor GmbH). The electrochemical setup consisted of a two-electrode configuration using a Pt foil as the counter electrode, and Ti foils as the working electrodes. TNTs with different thicknesses (1, 5, 20 μm) were fabricated as follows: 1) ~ 1μm thick nanotube layers with ~80 nm inner tube diameter in 50 vol.% glycerol + 50 vol.% H_2O + 0.27 M NH_4F at 20 V for 100 minutes [47, 48]; 2) ~5 μm thick nanotube layers with ~230 nm inner tube diameter in ethylene glycol + 10 vol.% H_2O + 150 mM NH_4F at 100 V for 4 h [48]; 3) ~20 μm thick nanotube layers with ~110 nm inner tube diameter in ethylene glycol + 1.5 vol.% H_2O + 176 mM NH_4F at 60 V for 4 h [49]. The aspect ratio (AR, equals to thickness/diameter ratio) of prepared TNTs was ~ 12, ~ 22 and ~ 180, respectively. All solutions were prepared from reagent grade chemicals. After anodization, all nanotube layers were rinsed and sonicated in isopropanol and dried in air, and further annealed in a muffle furnace at 400 °C for 1 h at a heating rate of 2.1 °C/min.

2.2 Decoration of anodic TNTs with Pt nanoparticles using ALD

The annealed anodic TNTs were homogeneously decorated with Pt nanoparticles by atomic layer deposition (thermal ALD, TFS 200, Beneq). The deposition processes were carried out at 300 ^oC by applying a different number of ALD cycles (N_{ALD}): 24, 40, 56, 72 88 and 104. (Trimethyl)methylcyclopentadienylplatinum(IV) (Sigma-Aldrich, 99%) and oxygen (Messer, 99.999%) were used as precursors. The Pt precursor was heated up to 80 ^oC and N_2 (99.9999%) was used as carrier gas at a flow rate of 500 standard cubic centimeters per minute (sccm). Under

these conditions, one ALD deposition cycle was defined by the following sequence: Pt precursor pulse (1s) - N_2 purge (5s) - O_2 pulse (1.5s) - N_2 purge (5s). All the resulted ALD Pt/TNT heterostructures are named as 1µm 24Cy Pt/TNT, 1µm 40Cy Pt/TNT etc., based on the nanotube length (here, 1 µm) and ALD cycle number (here, 24 and 40 cycles) depending on the different Pt/TNT samples. These notations are further used in the figures to distinguish the Pt/TNT samples. Two reference materials were used in this work for comparison using the same ALD process described above: i) flat TiO_2 layers obtained on the Ti foils (same as used for the anodization) by thermal annealing at 400°C for 1 hour, and ii) graphite sheets (Sigma-Aldrich) that were refluxed for 5 hours in nitric acid (65%) at 110^{o}C, sonicated in distilled water for 5 minutes and dried with nitrogen before the ALD process. In addition, commercial Pt/C powder (Sigma-Aldrich, content of Pt ≈5 wt. %) was grafted on the same type of graphite substrate from the alcoholic:nafion mixture (Nafion®117 solution, Sigma-Aldrich, content of Nafion ≈5 wt. %, 120 µl deposited per cm^2 of substrate area contained 12 mg of the powder) according to the previously published recipe [50]. Afterwards, it was dried at80°C for 3 hours and used for reference electrooxidation experiments without any other treatment.

2.3 Characterization of ALD Pt/TNT heterostructures

The structure, morphology, and size/distribution of Pt nanoparticle in ALD Pt/TNT samples was characterized by a field emission scanning electron microscopy (FE-SEM JEOL JSM 7500F) and a scanning transmission electron microscope (HR-TEM TITAN 60-300 with X-FEG type emission gun) equipped with Cs image corrector and a STEM high-angle annular dark-field detector (HAADF). The point resolution was 0.06 nm in TEM mode. The elemental mappings were obtained by STEM-Energy Dispersive X-ray Spectroscopy (EDS) with acquisition time 20 min. The quantitative elemental composition of Pt/TNTs was further evaluated using scanning

electron microscope (LYRA 3, Tescan) equipped with EDS analyzer AZtec X-Max 20 (Oxford Instruments) at acceleration voltage of 20 kV. The crystal structure of the ALD Pt/TNT was analyzed by diffraction analyses using X-ray diffractometer (Advance D8, Bruker AXE) using Cu Kα radiation with secondary graphite monochromatic and Na(Tl)I scintillation detector. Furthermore, X-ray photoelectron spectroscopy (XPS, PHI 5600) was used for analysis of composition and the chemical state of Pt. The diameters of Pt nanoparticles were measured and statistically evaluated using proprietary Nanomeasure software from the HR-TEM images. Average values and standard deviations were calculated from different samples/locations.

2.4 Electrocatalytic activity of ALD Pt/TNTs by methanol oxidation reaction

The as-prepared ALD Pt/TNT heterostructures were used as an electrocatalyst for methanol oxidation reaction (MOR) along with the reference materials described above. The electrocatalysis measurements were performed using an Autolab potentiostat (PGSTAT 204, Metrohm Autolab, Nova 1.10 software) with a conventional three-electrode system. The ALD Pt/TNT samples used as the working electrode, Pt wire served as the counter electrode and an Ag/AgCl electrode was used as the reference electrode. All potentials are reported against Ag/AgCl standard electrode potential. The cyclic voltammetry measurements (CV) were performed in the potential range from -0.1 to 0.8 V at a scan rate of 50 mV/s in sulphuric acid solution (1M H_2SO_4) with and without methanol (1M CH_3OH) addition under nitrogen (N_2) flow. All electrolyte solutions were purged with N_2 prior to CV measurements for 15 minutes to assure the removal of excess dissolved oxygen. In addition, the chronoamperometric (CA) performance of all the ALD Pt/TNT catalytic electrodes was investigated at the constant potential of 0.8 V for 7200 seconds with the N_2 flow.

3. Results and Discussion

Fig. 1 shows the FE-SEM images of the top and bottom views of ALD Pt/TNTs (N_{ALD} = 72) with 1, 5, 20 μm thick TNTs. The cross-sectional images of corresponding TNTs are shown in Fig. S1a-c. The average tube diameters of these tubes are ~80, 230 and 110 nm, respectively. It is obvious that the TNTs are homogeneously decorated with Pt nanoparticles within exteriors as well as interiors of TNTs for all thicknesses. However, at the very bottom parts of the nanotubes (i.e. at the interface with Ti substrates), many particle coalesce for $N_{ALD \geq}$ 56, especially outside the nanotubes (i.e. among the walls). This aspect will be discussed later. Fig. S1d shows XRD patterns of Pt/TNTs (N_{ALD} = 72, 20 μm thick TNTs) and corresponding blank TNTs (N_{ALD} = 0/non-decorated). The pattern of the blank TNTs and Pt/TNTs exhibits diffraction peaks of Ti (from the substrate) and crystalline anatase TiO_2 (PDF #04-002-8296). In Pt/TNT pattern for N_{ALD} = 72, diffraction peaks revealed at 2Θ=39.9, 46.3 and 67.7 (PDF # 04-001-3301) are ascribed to the Pt planes (111), (200) and (220) respectively.

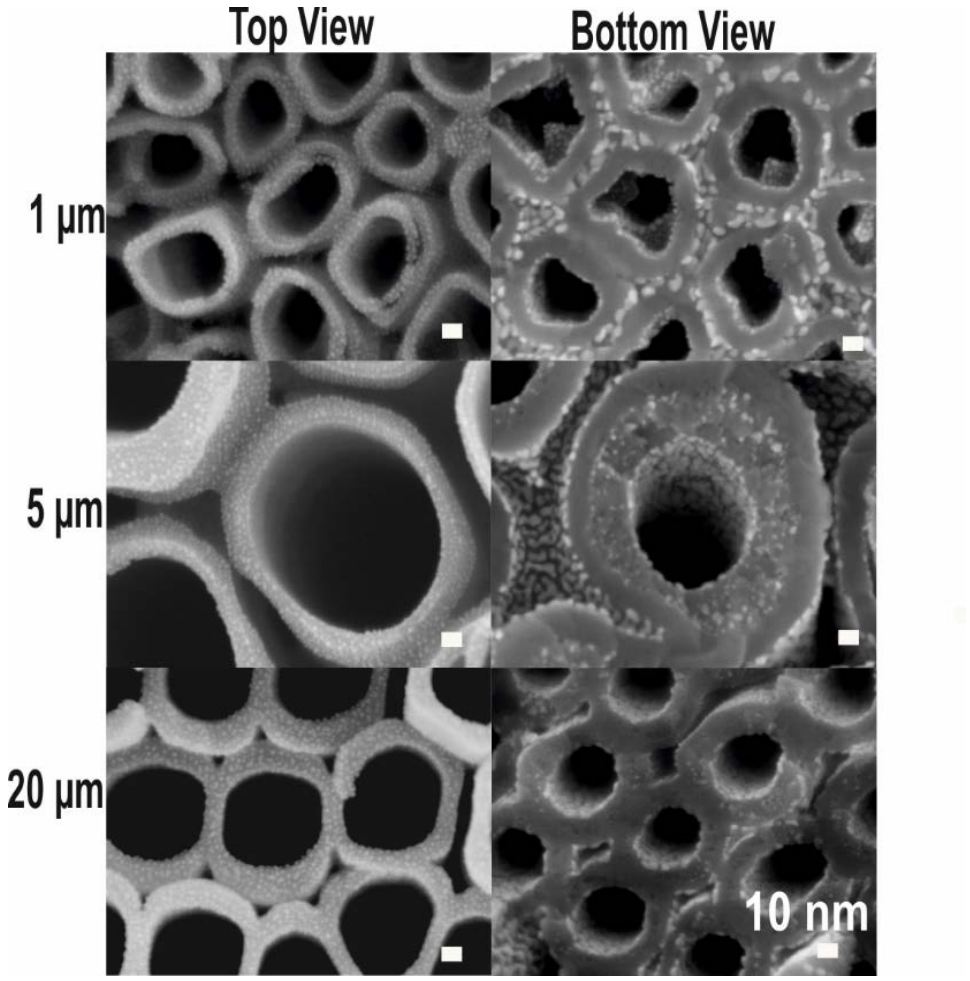

Fig.1. SEM images of the top and bottom views of Pt/TNTs with N_{ALD} = 72 of different thicknesses: 1 µm, 5 µm and 20 µm.

TEM analyses were carried out to further characterize the Pt-decorated nanotubes. Fig. 2 shows the TEM images Pt/TNTs of N_{ALD} = 0, 24, 40, 56 and 72 for 20 µm TNTs. Efforts were carried out to visualize also nanotube samples with N_{ALD} = 88 and 104. However, their imaging was not possible anymore as these nanotubes were not enough transparent for electrons. As one can see, there is an obvious absence of Pt nanoparticles for the N_{ALD} = 0 case. For decorated Pt/TNTs with N_{ALD} = 24, 40, 56 and 72, the particles are not only homogeneously distributed within the TNTs, but their diameter increases with increasing N_{ALD}. The TEM elemental

mapping shown in Fig. S2 further confirms homogenous Pt nanoparticle distribution within nanotubes.

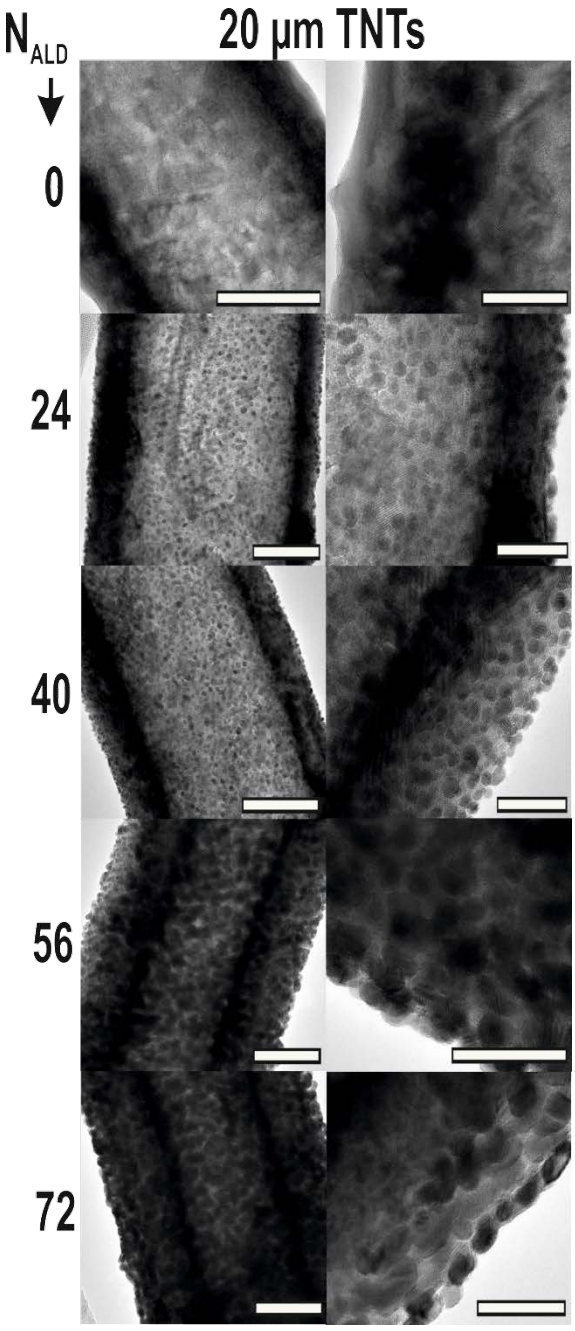

Fig.2. TEM images of 20 µm thick Pt/TNTs with N_{ALD} = 0, 24, 40, 56 and 72. The scale bars at left side (low magnification) and at the right side (higher magnification) images represent a distance of 50 nm and 20 nm, respectively.

The analysis of Pt nanoparticle size was carried out by SEM. It was found that the Pt particles were well separated for all types of TNTs all along their walls inside as well as outside. The only place where some coalescence was found was at the very bottom of the tubes in close vicinity of underlaying Ti substrates. This coalescence occurred for $N_{ALD \geq} 56$ and is a consequence of too many particles grown on too small and condensed area. Fig. 3 shows the summarized results of ALD cycle numbers vs. diameter of Pt nanoparticles analyses in ALD Pt/TNTs (20 μm thick), for which the bottom parts with coalesced particles were excluded, as they possess only very minor portion of the whole TNTs mass and volume. A linear increase of Pt nanoparticle diameter with increasing N_{ALD} was observed. The mean diameter of smallest particles (N_{ALD} = 24) is 1.3 nm, while the mean diameter of largest particles N_{ALD} = 88) is 4.6 nm. For the highest N_{ALD} (104), there are no more particles, but continuous coatings (as discussed later in more details), thus these data are not plotted in Fig. 3. These results are in accord with publications that report that discrete nuclei of Pt nanoparticles (average diameter lower than 2 nm) are formed for low cycle numbers in the initial stage of the process [41, 51]. Then with increasing ALD cycles the nuclei grow into discrete and well observable particles. After additional cycles, coalescence of particles comes into play. At even higher cycle numbers, the coalesced particles form island like or even continuous metallic films [41, 51]. After this initial growth, Pt nanoparticle decoration becomes clearly visible by SEM [52]. The nucleation delay that occurs during the initial ALD cycles of noble metals has been reported to be due to the lack of adsorption sites and/or large differences in the surface energy between substrate and noble metal. Thus, at lower cycles small nuclei are formed with lesser coverage on the surfaces. The details are explained in our previous report [52].

To provide some more evidence about the used samples, the cross-sectional SEM images of Pt/TNTs with N_{ALD} = 24, 40 and 56 for all thicknesses of TNTs are shown in Fig. S3 and high-magnification images of tubes of 20 thick TNT layer with N_{ALD} = 72, 88 and 104c are shown in Fig. S4. There are clearly less particles in the case of 88c, compared to 72c. However, the particles are of larger size for 88c. This must have an implication on the overall surface of the Pt catalyst, but not necessarily on its activity, which is significantly influenced also by the particle size. For the 104c case, the ALD process led to continuous metallic coating, because Pt nanoparticles already became large enough to fuse together. In any case, the Pt nanoparticles consisted of metallic Pt, as revealed from XPS measurements (Fig. S5).

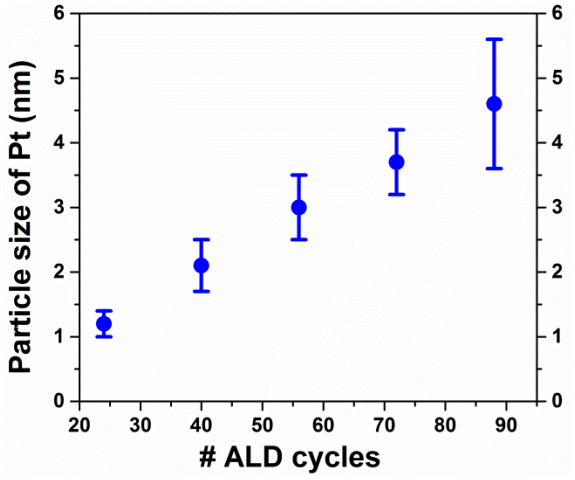

Fig. 3. Dependence of the Pt particle diameter on the number of ALD cycles (bottom parts of nanotubes with coalesced particles were excluded from this statistics).

The electrocatalytic performance of all the ALD Pt/TNT heterostructures with the corresponding blank (N_{ALD} = 0/non-decorated) TNTs toward methanol oxidation reaction (MOR) was evaluated. Fig. 4 shows the cyclic voltammograms (CV) for Pt/TNT catalyst electrodes of different ALD cycle numbers (0, 24, 40, 56, 72, 88, 104)/nanotube thickness (1, 5 and 20 μm) in

1 M H_2SO_4 solution with and without 1 M CH_3OH. Fig. 4(a-c) shows CVs obtained in 1 M H_2SO_4 (i.e. without methanol) in which, the hydrogen adsorption-desorption characteristic peaks around 0 V can be seen. These peaks were seen and extensively described in the literature [53, 54]. From the height of these peaks, it is possible to compare the electrochemical active area of Pt particles, which is for all nanotube layer thicknesses most pronounced for 72c. In Fig. 4c, additional oxidation and reduction peaks are seen in the range of 0.2 to 0.4 V, in particular for 72c. These peaks could be assigned to Pt oxidation and reduction [55], however, the overall picture does not speak for any events of this kind, since the samples with higher Pt loadings (which would cause even larger peaks) do not show these peaks so pronounced. These might be some specific sub-reactions that need to be investigated in detail in future work.

Fig. 4(d-f) shows CVs in 1 M H_2SO_4 + 1 M CH_3OH (i.e. with methanol) for all ALD Pt/TNT catalyst electrodes. As one can see, the anodic current density of methanol electro-oxidation increases with increasing TiO_2 nanotube layers thickness along with increasing ALD cycle numbers, except a discrepancy for N_{ALD} = 40 (which will be discussed later) for all types of Pt/TNT catalyst electrodes. The blank TNTs (N_{ALD} = 0) show the lowest response in all cases. It can be further seen from Fig. 4(d-f) that the substantial increase of current densities occurs for N_{ALD} = 56 and higher (compared to blank and N_{ALD} = 24, 40) for all types of Pt/TNTs. This is attributed to the presence of sufficient amount of well-distributed Pt nanoparticles with a suitable diameter for N_{ALD} = 56, 72, 88. Smaller particles (obtained for lower cycles) rendered significantly lower electrocatalytic activity. Similar observations were already reported previously [12, 30, 56, 57]. The maximum current densities obtained in MOR for all ALD Pt/TNTs with respect to ALD cycle numbers are given in Table 1. Among the experimental conditions used, the maximum performance of ~73.9 mA/cm^2 was achieved for N_{ALD} = 88 for

TNT layers with thickness of 20 μm, respectively. It was noted that the current density values in N_{ALD} = 40 were slightly lower than N_{ALD} = 24 for all types of TNTs, even though the corresponding particle diameter before electrochemical experiments was following the trend of linear increase with higher N_{ALD}. This difference can be ascribed to the coupling of Pt nanoparticles during methanol oxidation reaction (MOR) process. Bergamaski *et al* [50] reported that in order to understand the overall effect of particle diameter on electrocatalytic activity, the coupling among particles of different sizes in the nanometer range via soluble products must be considered.

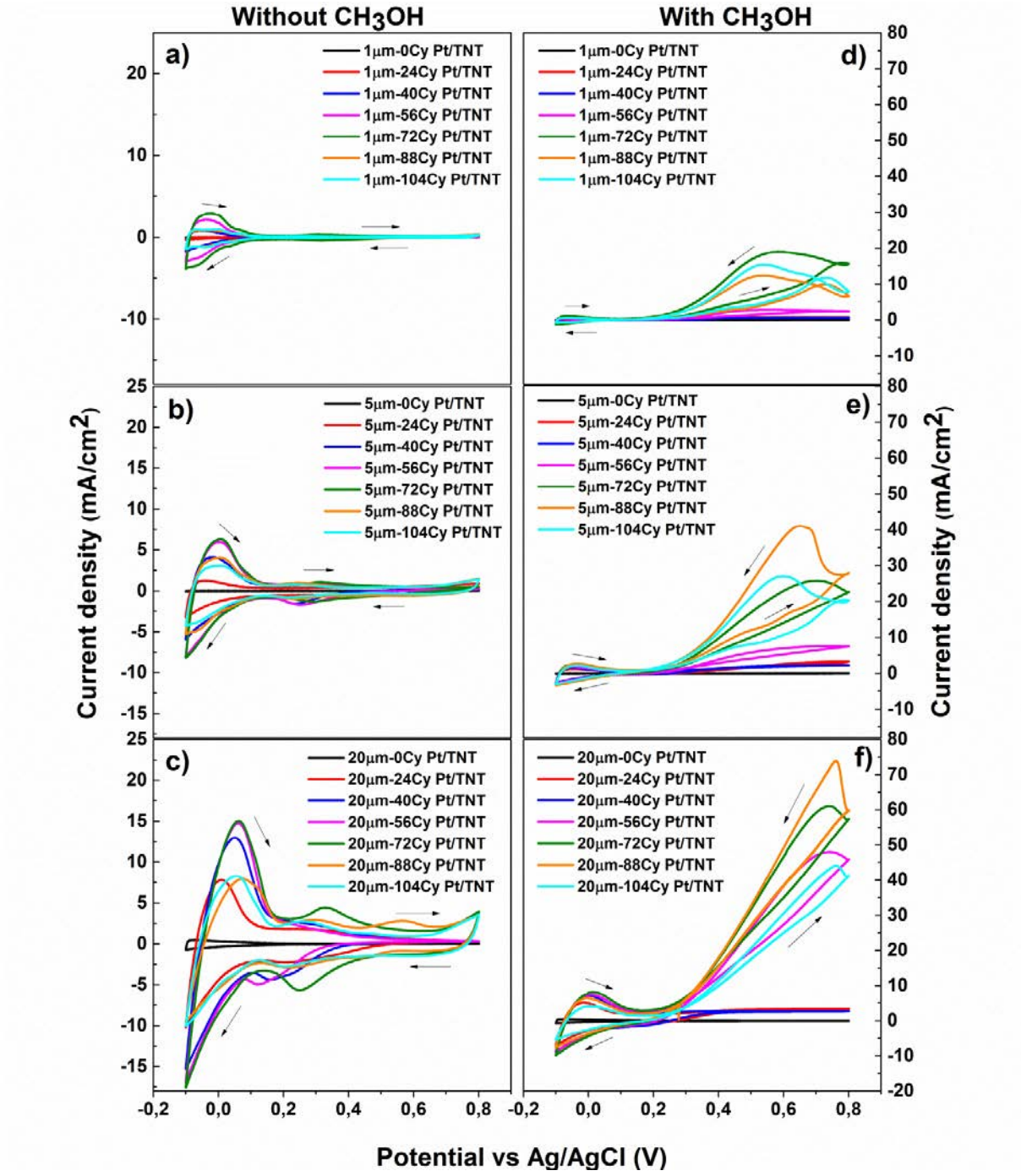

Fig. 4. Comparison of the cyclic voltammograms of different ALD Pt/TNT catalyst electrodes in 1M H_2SO_4 (without methanol, a-c) and in 1M H_2SO_4 +CH_3OH (with methanol, d-f) for 1, 5, 20 μm thick TNTs, at a scan rate of 50 mV/ s. Arrows indicate the direction of the CV scan.

In other words, it is necessary to determine the coupling of small and larger particles over distances on the order of nanometers during the MOR process, since the particle diameter distribution further influences the catalytic activity. Therefore, the lower efficiency for N_{ALD} = 40 can be mostly related to a partial oxidation of methanol due to lower mass activity of Pt particles.

TiO_2 Nanotube layer thickness (μm)	**ALD cycle numbers (N_{ALD})**	**Maximum current density (mA/cm^2) obtained in MOR**
1	24	0.75
	40	0.66
	56	2.7
	72	19
	88	12.4
	104	15.35
5	24	3.2
	40	2.3
	56	7.6
	72	25.75
	88	41
	104	27
20	24	3.35
	40	2.75
	56	47.9
	72	57.3
	88	73.9
	104	44

MOR=methanol oxidation reaction

Table 1. The maximum current densities obtained from CVs in Figure 4 for MOR for ALD Pt/TNTs with respect to TNT thicknesses/ALD cycle numbers (N_{ALD}).

However, the currents are relatively small for these low-cycle samples in general (regardless the thickness of the nanotube layer), so it could be considered as negligible phenomena for the scope of the present work.

A whole range of cyclic voltammograms was also recorded for the reference materials, as shown in Fig. S6-S8. Maximum currents obtained for these materials are summarized in Table S1. As one can see from these data, the electroxidation currents for any of these reference materials did not reach such high values as recorded for Pt/TNTs layers. The reason for Pt-graphite MOR current to be significantly higher for 72c than for the 88c is very straightforward – the 72c samples have Pt nanoparticles on the surface, while 88c has a complete Pt coating, which is limitedly active for MOR. It is known from the ALD field that the nature of substrates plays a large role for the nucleation and the growth rate of any deposited material. In this case, based on SEM investigation (not shown), the graphite is completely coated for the 88c, while nanotube layers still have Pt particles. In addition, onset potentials of ethanol electrooxidation were analyzed, as shown in Fig. S9. It turned out that they were all in the range of 0.2 -0.3 V.

In order to obtain additional information about the stability of the catalytic performance of Pt/TNTS and other reference materials, chronoamperometric measurements were carried out. Figure 5 shows chronoamperometric curves recorded for 20 μm thick TNT layers with various N_{ALD} at 0.8 V for 2 hours. In particular, the 88c Pt/ 20 μm TNT layers showed the highest currents (in line with CV curves shown in Fig. 4f) and superior stability over time, suggesting only very small poisoning of catalyst known from the literature [12, 54, 58]. Fig. S6c, S7c and S8c show chronoamperometric curves recorded for the corresponding reference substrates at 0.8V for 1 hour, after which already a significant decay of currents was observed. From all these

data it is clear that reference materials undergo significant poisoning in comparison with Pt/ TNT layers.

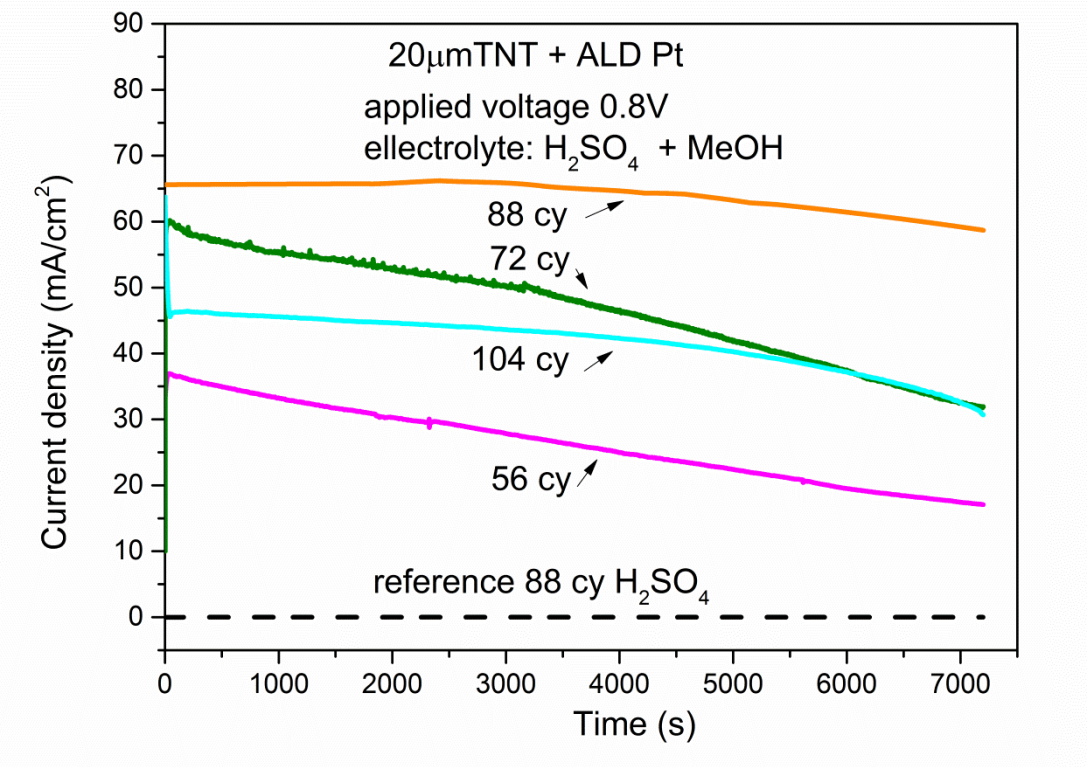

Fig.5. Chronoamperometric *i-t* curves for Pt/TNT with various N_{ALD} for 20 μm thick TNT layers in 1M H_2SO_4 +CH_3OH at 0.8V for 2 hours. Dashed curve shows one reference measurement under the same conditions but without CH_3OH.

In order to discuss the results, one has to keep in mind that the enhanced electrocatalytic activity of ALD Pt/TNT catalysts can be ascribed to the synergistic effect of Pt nanoparticle and TNT support. The bifunctional mechanism and electronic effect are the widely accepted models to account for the enhancement of electrocatalytic activity of the supported Pt catalysts [59, 60]. TiO_2 can stimulate CO tolerance through the bifunctional mechanism; also modify the electronic structure of Pt in terms of electronic effects. The bifunctional mechanism is used to describe how hydroxyl surface groups can oxidize and remove adjacent CO adspecies (CO_{ad}) from the Pt

catalyst surface, thus avoiding CO poisoning. Furthermore, the anatase TNT support of Pt nanoparticle can generate OH adspecies (OH_{ad}) during electrochemical processes, which can assist in removing CO like intermediates via oxidizing them, thereby reducing the poisoning of Pt catalyst [12, 58]. Due to the hydrophilic nature of TNTs, they are covered with hydroxyl groups in acidic electrolytes because of water dissociation on the TNT surface. The reaction steps of CO oxidation on Pt nanoparticles can be described by the following reaction equations [56, 59]:

$$TiO_2 + H_2O \rightarrow TiO_2 - OH + H^+ + e^- \quad (1)$$

$$Pt + CH_3OH \rightarrow Pt - CO_{ads} + 4H^+ + 4e^- \quad (2)$$

$$TiO_2 - OH + Pt - CO_{ads} \rightarrow CO_2 + Pt + TiO_2 + H^+ + e^- \quad (3)$$

$$Pt + H_2O \rightarrow Pt - OH + H^+ + e^- \quad (4)$$

$$Pt - CO_{ads} + Pt - OH \rightarrow 2Pt + CO_2 + H^+ + e^- \quad (5)$$

The electro-oxidation of CO should be considerably more favorable at the periphery of a Pt nanoparticle than in the inner area because of immediate contact of peripheral CO_{ad} with TiO_2–OH groups on the TNT support. As the immediate contact of CO_{ad} with TiO_2–OH group occurs at the periphery, the electro-oxidation of CO occurs predominantly at the periphery region of the Pt nanoparticles [59, 61]. The more free Pt sites become available, the rate of CO oxidation increases. However, there is also an influence of the dimensionality of the nanotubes coming from the unidirectional 1D shape of the nanotubes within their layers, where diffusional aspects come into play [47]. In order to assess this points, we provide in Table 2 a comparison of i) the surface area between TNTs (calculated from the dimensions of the NT and their number on 1

macroscopic cm^2) and the flat TiO_2 on Ti foil (which is essentially 1 cm^2 on 1 macroscopic cm^2 of the sample) and ii) current ratio between the maximum MOR currents (i.e. for N_{ALD} = 88c) obtained for corresponding Pt-TNTs (given in Table 1) and Pt-flat TiO_2 (which is 0.53 mA/cm^2, as shown in Table S1). As one can see, the current ratio is clearly higher over the surface area ratio for the 1 and 5 μm Pt/TNTs, which shows that the nanotubular shape in these cases is favourable for the MOR. However, for the 20 μm Pt/TNTs the surface area ratio is higher than the current ratio, which clearly shows that the entire available surface of these nanotubes cannot be any more effectively utilized, most likely due to diffusional issues (e.g. sterical hindrance of bubbles coming from the bottom parts of the tubes to the electrolyte, etc.). In other words, the pathway of some 10-20 μm is too long for reactants and products of MOR to travel effectively and quickly enough along the nanotube walls as for the 1 and 5 μm thick TNTs. Since the most favorable current over surface figure is achieved by the 5 thick Pt/TNTs, one can state that the 5 μm TNTs supported Pt/TNT catalyst electrodes can remove a larger portion of CO_{ad} species due to high surface area to volume ratio (availability of abundant Pt nanoparticles) and larger number ratio of peripheral Pt sites to the total surface sites than other TNT supports (1 and 20 μm).

TiO_2 Nanotube layer thickness (μm)	**Surface ratio (cm^2 of NT/cm^2 of flat TiO2)**	**MOR max current ratio (mA/cm^2 of Pt/TNT vs. mA/cm^2 of Pt-TiO_2 flat**
1	17	23
5	44	76
20	377	137

Table 2. Comparison of the surface area and MOR maximal currents between Pt/TNTs and Pt-TiO2 flat (assuming the total surface area of Pt- TiO_2 flat to be 1cm^2 on 1cm^2 of the sample).

In addition, in order to assess the performance and magnitude of the results of Pt/TNT catalyst presented in this work, it is necessary to compare the obtained results with similar materials in published literature. Table 3 summarizes the previous studies on the electrocatalytic performance of Pt nanoparticles deposited on TNTs by using various methods; considering Pt nanoparticles along with other nanoparticles.

Sample (Pt with various supports)	**Pt deposition method**	**Pt particle diameter (nm)**	**Max. current density (mA/cm^2)**	**Reference**
Pt/TNT	Hydrothermal reduction	46-200	11.75	[12]
Pt/TNT	Chemical impregnation	NR	2.72	[26]
Pt/TNT	Photo irradiation	5	21	[29]
Pt/TNT	Photo reduction	2-5	60	[30]
Pt/TNT	Thermal decomposition	50	3.65	[31]
Pt/TNT	ALD	1.3-4.6	74	This work

NR: not reported

Table 3. Comparison of the electrocatalytic activities of Pt/TNTs in methanol oxidation reaction based on previous reports.

From the Table 3 it can be seen that Pt nanoparticles with 2-5 nm diameter deposited by photoreduction method achieved highest electrocatalytic activity via electrochemical pretreatment of the Pt/TNT in H_2SO_4 for 800 cycles CV [30]. Dimension of those nanotubes are not given in that paper. However, in this study, significantly higher electrocatalytic activity compared to the published state-of-art was achieved without any pre-treatment.

4. Conclusions

In this study, anodic TNT layers with three different thicknesses (1, 5 and 20 μm) were homogeneously decorated with Pt nanoparticles using atomic layer deposition (ALD) and different numbers of ALD cycles (N_{ALD} = 24, 40, 56, 72, 88 and 104). The Pt decorated Pt/TNTs were further used as electrocatalysts for methanol oxidation reaction (MOR). The Pt particle diameter increased linearly with increasing N_{ALD}. The maximum electrocatalytic performance was obtained for 20 μm thick TNT layer decorated by Pt particles of an average diameter of 4.6 nm (using ALD with 88 cycles) showing 74 mA/cm^2 of anodic current density with excellent time stability. All reference materials showed lower MOR catalytic activity in general and also significant decrease of MOR catalytic activity in time due to the poisoning of the catalyst. The effective utilization of high aspect ratio anodic TNT layers as catalyst supports and the optimal utilization of Pt nanoparticles for enhanced electrocatalytic activities can be achieved via homogeneous distribution of Pt using ALD process.

Acknowledgements

The authors gratefully acknowledge support from the European Research Council (ERC, project No. 638857) and the Ministry of Education, Youth and Sports of the Czech Republic (projects LM2015082 and CZ.02.1.01/0.0/0.0/16_013/0001829, LQ1601). We thank Dr. Veronika Podzemna, Assoc. Prof. Ludvík Beneš and Dr. Klára Čepé (RCPTM, Olomouc) for SEM, XRD and TEM analyses, respectively.

References

[1] A. M. Zainoodin, S. K. Kamarudin, W. R. W. Daud, Int. J. Hydrogen Energy 35 (2010) 4606.

[2] P.N. Ross Jr., H.A. Gasteiger, in: O. Savadogo (Ed.), New Materials for Fuel Cells Systems 1, Editions de L'Ecole Polytechnique de Montreal, 1995.

[3] A. S. Aricò, S.Srinivasan, V. Antonucci, Fuel Cells 1 (2011) 133.

[4] H. J. Huang, X.Wang, J. Mater. Chem. A 2 (2014) 6266.

[5] H. S. Liu, C. J. Song, L.Zhang, H. J. Wang, D. P. Wilkinson, J. Power Sources 155 (2006) 95.

[6] X. Zhao, M. Yin, L. Ma, L. Liang, C. Liu, J. Liao, T. Lu, W. Xing, Energy Environ. Sci. 4 (2011) 2736.

[7] M. N. Cao, D. S. Wu, Cao, R. ChemCatChem 6 (2014) 26.

[8] N. Kizhakevariam, E. M. Stuve, Surf. Sci. 286 (1993) 246.

[9] R.N. Singh, R. Awasthi, C.S. Sharma, Int. J. Electrochem. Sci. 9 (2014) 5607.

[10] A. Guerro-Ruiz, P. Badenes, I. Rodriguez-Ramos, Appl Catal A: Gen 173 (1998) 313.

[11] J.M. Leger, C. Lamy, Ber. Bunsen-Ges. Phys. Chem. 94 (1990) 1021.

[12] K. R. Rasmi, S. C. Vanithakumari, R. P. George, C. Mallika, U. Kamachi Mudali, RSC Adv. 5 (2015) 108050.

[13] T. Shu, S. Liao, C.-T. Hseih, W.-Y Chen, Electrochim. Acta 75 (2012) 101.

[14] Y. Wang, J. Clancey, G. Lu, J. Liu, L. Liu, J. Chaudhuri, S. George, M. Xie, S. Wei, Z. Guo, J. Electrochem. Soc. 163 (2016) F1.

[15] S. J. Tauster, S. C.Fung, R. L. Garten, J. Am. Chem. Soc. 100 (1978) 170.

[16] C. Jackson, G. T. Smith, D. W. Inwood, A. S. Leach, P. S. Whalley, M. Callisti, T. Polcar, A. E. Russell, P.Levecque1, D. Kramer, Nat. Commun. 8 (2017) 15802.

[17] I. Paramasivam, H. Jha, N. Liu, P. Schmuki, Small 8 **(**2012) 3073.

[18] Q. Lv, M. Yin, X. Zhao, C.P. Liu, W. Xing, J. Power Sources 218 (2012) 93.

[19] Y. J. Ko, H. S. Oh, H. Kim, J. Power Sources 195 (2010) 2623.

[20] Z. Q. Yao, M. S. Zhu, F. X. Jiang, Y. K. Du, C. Y. Wang, P.Yang, J. Mater. Chem. 22 (2012) 13707.

[21] L. Xing, J. B. Jia, Y. Z. Wang, B. L. Zhang, S. J. Dong, Int. J. Hydrogen Energy 35 (2010) 12169.

[22] H. Sopha,T. Samoril, E. Palesch, L. Hromadko, R. Zazpe, D. Skoda, M. Urbanek, S. Ng, J. Prikryl, J.M. Macak, Chemistry Open 6 (2017) 480.

[23] H. Feng, Y. Liang, K. Guo, W. Chen, D. Shen, L. Huang, Y. Zhou, M. Wang, Y. Long, Environ. Sci. Technol. Lett. 3 (2016) 420.

[24] J.M. Macak, H. Tsuchiya, A. Ghicov, K. Yasuda, R. Hahn, S. Bauer, P. Schmuki, Curr. Opin. Solid State Mater. Sci. 11 (2007) 3.

[25] K. Lee, A. Mazare, P. Schmuki, Chem. Rev. 114 (2014) 9385.

[26] M. Manikandan, R. Vedarajan, R. Kodiyath, H. Abe, S. Ueda, A. Dakshnamoorthy, N. Rajalakshmi, K. S. Dhathathreyan, G. V. Ramesh, J. Nanosci. Nanotechnol. 16 (2016) 8269.

[27] Y. Yin, X. Tan, F. Hou, L. Zhao, Front. Chem. Eng. China 3 (2009) 298.

[28] J.M. Macak, P.J. Barczuk, H. Tsuchiya, M.Z. Nowakowska, A. Ghicov, M. Chojak, S. Bauer, S. Virtanen, P.J. Kulesza, P. Schmuki, Electrochem. Commun. 7 (2005) 1417.

[29] Y.-Y. Song, Z.-D. Gao, P. Schmuki, Electrochem. Commun. 13 (2011) 290.

[30] M. Tian, G. Wu, A. Chen, ACS Catal. 2 (2012) 425.

[31] Y. Luo, S. Xu, W. Zhong , Z. Xiao, Adv Mat Res. 750-752 (2013) 1696.

[32] S.N. Basahel, K.Lee, R.hahn, P.Schmuki, S.M. Bawaked, S.A. Al-Thabaiti, Chem.Commun. 50 (2014) 6123.

[33] N.R. Nguyen, J.Yoo, M.Altomare, P.Schmuki, Chem.Commun. 50 (2014) 9653.

[34] J. R. C. Salgado, F. Alcaide, G. ´A lvarez, L. Calvillo, M. J. L´azaro, E. Pastor, J. Power Sources 195 (2010) 4022.

[35] K. Koczkur, Q. Yi, A. Chen, Adv. Mater. 19 (2007) 2648.

[36] L. Wang, Y. Yamauchi, J. Am. Chem. Soc. 135 (2013) 16762.

[37] C. Cheng, H. Zhang, W. Ren, W. Dong, Y. Sun, Nano Energy 2 (2013) 779.

[38] E. Rikkinen, A. Santasalo-Aarnio, S. Airaksinen, M. Borghei, V. Viitanen, J. Sainio, E. I. Kauppinen, T. Kallio, A. O. I. Krause, J. Phys. Chem. C 115 (2011) 23067.

[39] F. Grillo, H.V. Bui, J. A. Moulijn, M. T. Kreutzer, J. R. van Ommen, J. Phys. Chem. Lett. 8 (2017) 975.

[40] J. Lu, J. W. Elam, P. C. Stair, Acc. Chem. Res. 46 (2013) 1806.

[41] H. Zhang, C. Cheng, J. Mater. Chem. A 4 (2016) 15961.

[42] Y. Wang, J. Clancey, G. Lu, J. Liu, L. Liu, J. Chaudhuri, S. George, M. Xie, S. Wei, Z. Guo, J. Electrochem. Soc.163 (2016) F1.

[43] M. B. E. Griffiths, P. J. Pallister, D. J. Mandia, S. T. Barry, Chem. Mater. 28 (2016) 44.

[44] M. Mäkelä, T. Hatanpää, K. Mizohata, J. Räisänen, M. Ritala, M. Leskelä, Chem. Mater. 29 (2017**)** 6130.

[45] H. Feng, J. W. Elam, J. A. Libera, W. Setthapun, P. C. Stair, Chem. Mater. 22 (2010) 3133.

[46] L. Assaud, N. Brazeau, M. K. S. Barr, M. Hanbücken, S. Ntais, E.A. Baranova, L. Santinacci, ACS Appl. Mater. Interfaces 7 (2015) 24533.

[47] J. M. Macak, H. Hildebrand, U. Marten-Jans, P. Schmuki, J. Electroanal. Chem. 621 (2008) 254.

[48] S. Das, H. Sopha, M. Krbal, R. Zazpe, V. Podzemna, J. Prikryl, J.M. Macak. ChemElectroChem 4 (2017) 1.

[49] R. Zazpe, M. Knaut, H. Sopha, L. Hromadko, M. Albert, J. Prikryl, V. Gärtnerová, J.W. Bartha, Langmuir 32 (2016) 10551.

[50] K. Bergamaski, A.L. N. Pinheiro, E. Teixeira-Neto, F. C.Nart, J. Phys. Chem. B 110 (2006) 19271-19279.

[51] D. M. Hausmann, R. G. Gordon, J. Cryst. Growth 249 (2003) 251.

[52] J. Yoo, R. Zazpe, G. Cha, J. Prikryl, I. Hwang, J. M. Macak, P. Schmuki, Electrochem. Commun., 86 (2018) 6-11.

[53] K. Kinoshita, J. Lundquist, P. Stonehart, J. Catal. 31 (1973) 325

[54] Ch. L. Childers, H. Huang, C. Korzeniewski, Langmuir, 15 (1999) 786.

[55] M. Umeda, M. Kokubo, M. Mohamedi, I. Uchida, Electrochim. Acta 48 (2003) 1367

[56] C.-C. Ting, C.-H. Liu, C.-Y. Tai, S.-C. Hsu, C.-S. Chao, F.-M.Pan, J. Power Sources 280 (2015) 166.

[57] T. Frelink, W. Visscher, J.A.R. van Veen, J. Electroanal. Chem. 382 (1995) 65.

[58] O.V. Cherstiouk, P.A. Simonov, E.R. Savinova, Electrochim. Acta 48 (2003) 3851

[59] C. S. Chen, F. M. Pan, Appl. Catal. B- Envir. 91 (2009) 663.

[60] Z. Jusys, H. Massong, H. Baltruschat, J. Electrochem. Soc. 146 (1999) 1093.

[61] C.-C. Ting, C.-H. Chao, C. Y. Tsai, I-K. Cheng, F.-M. Pan, Appl. Surf. Sci. 416 (2017) 365.